THE JOURNAL OF PHYSICAL CHEMISTRY C

Article

Cite This: J. Phys. Chem. C 2018, 122, 670−680

pubs.acs.org/JPCC

Silver Valence State Determines the Water Tolerance of Ag/Al_2O_3 for the $H_2−C_3H_6−SCR$ of NO_x

Guangyan Xu,[†,‡] Yunbo Yu,*[,†,‡,§] and Hong He*[,†,‡,§]

[†]State Key Joint Laboratory of Environment Simulation and Pollution Control, Research Center for Eco-Environmental Sciences, Chinese Academy of Sciences, Beijing 100085, China

[‡]University of Chinese Academy of Sciences, Beijing 100049, China

[§]Center for Excellence in Regional Atmospheric Environment, Institute of Urban Environment, Chinese Academy of Sciences, Xiamen 361021, China

Supporting Information

ABSTRACT: The influence of the silver valence state on Ag/Al_2O_3 on the water tolerance of $H_2−C_3H_6−SCR$ of NO_x was investigated. The valence state of silver species on Ag/Al_2O_3, which was carefully characterized by XPS, UV−vis, and XANES measurements, was adjusted by varying the calcination temperature from 500 to 900 °C. Oxidized silver species were predominant on Ag/Al_2O_3 calcined at temperatures below 600 °C (LT-catalysts), while further increasing the calcination (temperatures above 600 °C, HT-catalysts) promoted the transformation of oxidized silver species into metallic silver clusters. The samples with higher amounts of oxidized silver species exhibited better water tolerance in the $H_2−C_3H_6−SCR$. Activation energy measurements confirmed that the mechanism of NO_x reduction on these catalysts was the same. In situ DRIFTS studies demonstrated that metallic silver species promoted the formation of active enolic species and the complete oxidation of formate, thus improving the low-temperature activity of HT-catalysts in the absence of water vapor. Water addition eliminated the formate, releasing the active Ag^+ sites for enolic species formation, and thus promoted the low-temperature activity of LT-catalysts. From a comprehensive point of view, 60% oxidized silver species on Ag/Al_2O_3 catalysts is the optimal percentage for $deNO_x$ performance and water tolerance.

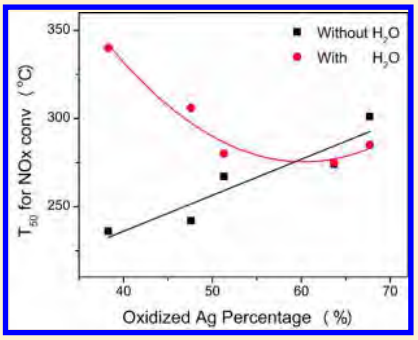

1. INTRODUCTION

Nitrogen oxides (NO_x) emission from diesel engines is one of the main sources of air pollution, such as acid rain, photochemical smog and haze. For diesel engine exhaust purification, various technologies have been developed for NO_x removal, among which selective catalytic reduction utilizing hydrocarbons (HC−SCR) would be an elegant alternative to the $NH_3−SCR$ and the lean NO_x trap (LNT) technologies.[1−3] Up to now, different kinds of catalysts have been created for HC−SCR, among which Ag/Al_2O_3 is widely accepted as one of the most promising catalysts.[1−3] During the HC−SCR process, however, Ag/Al_2O_3 usually exhibits high efficiency for NO_x conversion at temperatures above 400 °C, which is higher than the typical temperatures of diesel engine exhaust, still being inadequate for practical applicantion.[1]

Since the pioneering work of Miyadera,[4] many efforts have been made to enhance the $deNO_x$ activity of Ag/Al_2O_3 in HC−SCR, focusing on the Ag content and state, properties of the Al_2O_3 support, preparation method, structure of hydrocarbons, and the promotion effect of hydrogen.[5−15] Over the Ag/Al_2O_3 catalysts, it was confirmed that the active components of Ag mainly comprised silver cations (Ag^+), oxidized silver clusters ($Ag_n^{\delta+}$), and metallic silver clusters (Ag_n^0),[1−3,10] among which the oxidized silver species (Ag^+ and $Ag_n^{\delta+}$) were active for NO_x reduction.[1−3,16−18] As for the Ag/Al_2O_3 catalysts with 2−4 wt % Ag loading, oxidized silver species were predominant, exhibiting high activity for HC−SCR.[1−3,19] More recently, a relationship between NO_x uptake measured by TPD and Ag surface density/Ag loading was clearly drawn by Thomas and co-workers,[5,6] and the obtained optimum silver surface density was related to the $deNO_x$ performance of $C_3H_6−SCR$. It was also reported that metallic Ag promoted the partial oxidation of hydrocarbons (HCs), enhancing the HC−SCR process at low temperatures, and thus an optimal surface metallic/oxidized Ag ratio is probably needed for best performance.[9,13,14]

Zhang et al.[20] synthesized Ag/Al_2O_3 catalysts utilizing several precursors of Al_2O_3, and reported that the catalyst derived from AlOOH exhibited the best $C_3H_6−SCR$ activity, mainly due to the high density of Ag−O−Al entities. Ag/Al_2O_3 catalysts were synthesized by Luo et al.[21] via impregnation, coprecipitation, and single sol−gel methods, among which the catalyst prepared by sol−gel exhibited the optimal surface area and Ag species dispersion, and thus showed the highest $deNO_x$ activity. Shimizu et al. investigated the influence of reductant structure on the $deNO_x$ activity of $Ag−Al_2O_3$, and proposed

Received: November 3, 2017
Revised: December 12, 2017
Published: December 15, 2017

DOI: 10.1021/acs.jpcc.7b10860
J. Phys. Chem. C 2018, 122, 670−680

that the catalytic performance and water resistance were significantly improved by the increase of the carbon number of alkane reductant.[15]

The discovery of the "hydrogen effect," meaning that hydrogen significantly promotes the low-temperature activity of Ag/Al_2O_3 catalysts, brings the HC−SCR closer to practical application.[22,23] During the past decade, many research groups committed to comprehending the "hydrogen effect" on HC−SCR over silver catalysts.[3,10,24−26] Though there remains some debate on the origin of the "hydrogen effect", it is generally believed that H_2 addition promotes the partial oxidation of hydrocarbons to produce active intermediates, thus enhancing NO_x reduction activity.[3,6,12,24,27,28] In addition, in situ catalytic reforming of diesel or its additive to produce hydrogen will be a viable method for obtaining hydrogen.[29,30]

It should be highlighted that the above achievements involving the design of silver catalysts with high efficiency for HC−SCR were often obtained without H_2O in the feed. Considering that H_2O is inevitably present in diesel engine exhausts, the design of catalysts with excellent water resistance is therefore highly desired for practical application. More recently, we found that the water tolerance of Ag/Al_2O_3 in $H_2-C_3H_6$−SCR was governed by silver loading.[31] To further reveal intrinsic properties determining the water tolerance of silver catalysts for HC−SCR, herein, the silver loading of 2 wt % was employed, while the silver valence state was adjusted by varying the calcination temperature. Based on UV−vis and XPS measurements, a quantitative relationship between the percentage of oxidized silver species on Ag/Al_2O_3 and water tolerance was revealed, providing a new insight into understanding the water tolerance of silver catalysts during the HC−SCR reaction.

2. MATERIALS AND METHODS

2.1. Catalyst Synthesis and Characterization. The 2 wt % Ag/Al_2O_3 catalysts were synthesized by the impregnation method, utilizing silver nitrate (AR) and boehmite (SASOL, SB-1) as the precursors.[2,24,32] After impregnation, the samples were put in a rotary evaporator to remove the surplus water. The samples were then calcined in air at 500, 600, 700, 800, and 900 °C for 3 h, respectively (thereafter denoted as Ag-500, Ag-600, Ag-700, Ag-800, and Ag-900, respectively). Meanwhile, Ag-500 and Ag-600 were defined as LT-catalysts, and Ag-800 and Ag-900 were defined as HT-catalysts. A pure Al_2O_3 sample was also prepared and calcined at 600 °C by the same procedure, with boehmite as the precursor.

The BET surface area was measured utilizing a Quantachrome Autosorb-1C instrument at 77 K. X-ray powder diffraction (XRD) experiments were performed on a Rigaku D/max-RB X-ray diffractometer (Japan) utilizing Cu Kα radiation in the 2θ range from 10° to 90°.

XPS measurements were carried out on a scanning X-ray microprobe (PHI Quantera, ULVAC-PHI, Inc.) with Al Kα radiation at a step size of 0.1 eV, using C 1s (284.8 eV) as reference. UV−vis measurement were performed in absorption mode on a UV−vis spectrophotometer (Hitachi, U3100, Japan), using Al_2O_3 as reference for the baseline spectrum.

XANES analyses of the Ag−K edges were carried out in transmission mode at the BL14W1 XAFS beamline at the Shanghai Synchrotron Radiation Facility (SSRF). The PE storage ring operates at 3.5 GeV with an average storage current of 200 mA. Data presented here were analyzed with the Athena program.[33]

2.2. Catalyst Activity Test. Catalytic activity tests were performed in a fixed-bed flow quartz reactor (7 mm i.d.) by stepwise increase of the temperature. The reaction mixture was fed as follows: NO 800 ppm, C_3H_6 1714 ppm, H_2 1%, O_2 10%, H_2O 10% (if added) in N_2 balance at a total flow of 1000 mL/min, which was equivalent to a gas hourly space velocity (GHSV) of 100 000 h^{-1} (ca. 0.3 g catalyst).[31,34] Water vapor was precisely controlled by a micropump and vaporized prior to introduction into the reaction system. To avoid water condensation, both the gas line and the gas cell of the FTIR spectrometer were heated to 120 °C. The concentrations of NO, NO_2, NH_3, N_2O, and C_3H_6 were analyzed online with an FTIR spectrometer (Nicolet Nexus is10).[34−36] Conversions of NO_x and C_3H_6 were calculated as follows:

$$NO_x \text{ conversion} = \frac{[NO_x]_{in} - [NO_x]_{out}}{[NO_x]_{in}} \times 100\% \quad (1)$$

$$C_3H_6 \text{ conversion} = \frac{[C_3H_6]_{in} - [C_3H_6]_{out}}{[C_3H_6]_{in}} \times 100\% \quad (2)$$

where $NO_x = NO + NO_2$.

2.3. Activation Energy Measurement. The apparent activation energy (E_a) of NO_x was measured in the fixed-bed reactor as described above. On the basis of our previous work,[31] catalysts with a particle size of 0.45−0.9 mm were used for kinetic measurements. The weight of catalysts was adjusted with the GHSV varying from 150 000 to 600 000 h^{-1} in order to keep NO_x conversion below 20%. Prior to the kinetic measurements, all catalysts were calcined in 10% O_2/N_2 at 450 °C for 30 min.

According to previous studies,[31,34] the reaction rates of NO_x conversion ($-R_{NO_x}$) can be calculated from the kinetic data as follow:

$$-R_{NO_x} \text{ (mol/g/s)} = F_{NO_x} \times X_{NO_x}/W \quad (3)$$

where F_{NO_x} is the molar flow rate of NO_x (mol/s), X_{NO_x} is the conversion of NO_x, and W is the weight of catalyst. According to the above results, the Arrhenius plots for NO_x reduction were drawn, and then the related activation energies were obtained from the slope of the plots.

2.4. In Situ DRIFTS Studies. In situ DRIFTS measurements were carried out on a Nexus 670 (Thermo Nicolet) FT-IR, utilizing a MCT/A detector. Water vapor (5%) was supplied by passing the gas flow over a water bottle, with the gas line heated to 120 °C to prevent moisture condensation. Before the experiment, the samples were calcined in 10% O_2/N_2 flow (300 mL/min) at 450 °C for 30 min, and subsequently cooled to target temperature to obtain a spectrum for reference (30 scans, resolution of 4 cm^{-1}). DRIFTS spectra were collected under a stream of reactive gas flow.

3. RESULTS AND DISCUSSION

3.1. Structural Properties of Ag/Al_2O_3 Catalysts. Ag/Al_2O_3 catalysts calcined at different temperatures and pure γ-Al_2O_3 were characterized with BET and XRD tests, with results shown in Table 1 and Figure S1. The pure γ-Al_2O_3 had a specific surface area of 214 m^2/g and pore diameter of 10.5 nm. The LT-catalysts exhibited surface areas similar to that of pure γ-Al_2O_3, varying from 236 to 206 m^2/g, while high temperature calcination (up to 800 °C) resulted in a decrease in the surface area and an increase in the average pore size.

DOI: 10.1021/acs.jpcc.7b10860
J. Phys. Chem. C 2018, 122, 670−680

Table 1. Structural Parameters of Pure γ-Al_2O_3 Calcined at 600 °C and Ag/Al_2O_3 Catalysts Calcined at Different Temperatures

sample	BET surface area (m^2/g)	pore volume (cm^3/g)	average pore size (nm)
γ-Al_2O_3	214	0.561	10.5
Ag-500	236	0.527	8.92
Ag-600	206	0.536	10.4
Ag-700	208	0.551	10.8
Ag-800	155	0.517	13.3
Ag-900	151	0.535	14.2

As revealed by XRD patterns (Figure S1), Ag/Al_2O_3 calcined at temperatures below 700 °C showed phases similar to the pure Al_2O_3, for which only the γ-Al_2O_3 phase (2θ = 37.2°, 45.8°, and 66.9°) was observed. As the calcination temperature further increased, the δ-Al_2O_3 phase (2θ = 32.7°) was also observed for Ag-800 and Ag-900. Such transformation of Al_2O_3 resulted in an obvious decrease of BET surface area, which was also observed in previous study.[13] Meanwhile, no silver phase was detected in any of the samples, indicating that the silver species was highly dispersed or did not form a crystalline silver phase.[13,37]

The valence state of Ag supported on Al_2O_3 was characterized by UV−vis analysis, with results shown in Figure 1. To eliminate the interference of Al_2O_3 absorption, the

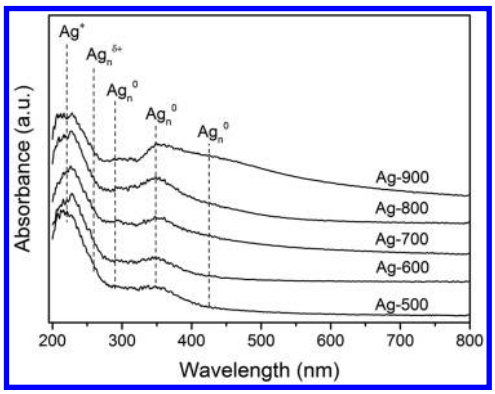

Figure 1. UV−vis spectra of Ag/Al_2O_3 calcined at different temperatures.

spectrum of pure Al_2O_3 has been subtracted from those of the Ag/Al_2O_3 catalysts. Five absorption peaks were observed at 220, 260, 290, 350, and 425 nm. The peak centered at 220 nm is generally assigned to the highly dispersed silver cations (Ag^+), and the band at 260 nm is commonly attributed to oxidized Ag cluster ($Ag_n^{\delta+}$). Meanwhile, metallic silver species (Ag_n^0) generally emerge at 290, 350, and 425 nm.[37−40] On the LT-catalysts, the band at 220 nm exhibited the highest intensity, indicating that the highly dispersed silver cations were predominant.[34] As the catalyst calcination temperature increased, however, the bands at 350 and 425 nm were significantly enhanced, accompanied by a weakening of the band at 220 nm.

For quantitative comparison of these silver species on the series of Ag/Al_2O_3 samples calcined at distinct temperatures, the UV−vis spectra were further fitted and deconvoluted to the constituent bands,[34] with the results shown in Figure S2 and Table 2. On the basis of the fitting results, oxidized silver species (Ag^+ and $Ag_n^{\delta+}$) accounted for 67.7% of the total silver species on the surface of Ag-500. High temperature calcination resulted in a decrease in the percentage of oxidized silver species from 63.7% to 38.3% (from 600 to 900 °C). These results confirmed that increasing calcination temperature promoted the transformation of oxidized silver species into metallic silver clusters.

The XPS measurement was further performed to confirm the valence states of silver supported on the Al_2O_3. As shown in Figure S3A, the Ag $3d_{5/2}$ binding energy bands were located at 367.7−368.4 eV, which was in accordance with the literature.[31,34,36] In order to obtain more information about the valence states, the XPS spectra were fitted and deconvoluted to the constituent bands (Figure S3B and Table S1).[38,41,42] On the surface of Ag-500, 71.3% of silver was present as oxidized silver species, consistent with the UV−vis results. Also, the increase in calcination temperature gradually decreased the percentage of oxidized silver species, further confirming the critical role of calcination temperature in determining the valence state of silver (Table 3).

To obtain a better understanding of the precise chemical state of silver supported on the Al_2O_3, the Ag−K XANES of Ag/Al_2O_3 catalysts, Ag foil, and $AgNO_3$ were measured (Figure S4). The first-order derivative peaks for $AgNO_3$ and Ag foil were observed at 25518.3 and 25515.3 eV, respectively. The corresponding peaks for the Ag/Al_2O_3 catalysts calcined at gradually increasing temperatures appeared at 25517.0, 25517.5, 25516.8, 25516.7, and 25515.9 eV, respectively. Obviously, the Ag/Al_2O_3 catalysts exhibited similar Ag−K absorption edge energies to that of $AgNO_3$, which was higher than that of Ag foil. These results further demonstrated that oxidized silver species were predominant on the LT-catalysts, while increase of the calcination temperature promoted the transformation of some oxidized silver to metallic silver clusters.

3.2. Influence of Water Vapor on the deNO$_x$ Performance. The deNO$_x$ performance and water tolerance of Ag/Al_2O_3 catalysts calcined at different temperatures were

Table 2. Percentage of Different Silver Species Calculated by Analysis of the Integrated Peak Area of the Deconvoluted UV−Vis Spectra

	percentage of silver species (%)				
sample	Ag^+ (220 nm)(25)[a]	$Ag_n^{\delta+}$ (260 nm)(10)[a]	Ag_n^0 (290 nm)(20)[a]	Ag_n^0 (350 nm)(35)[a]	Ag_n^0 (425 nm)(40)[a]
Ag-500	66.5	1.2	7.7	21.3	3.2
Ag-600	62.8	0.9	7.5	25.1	3.6
Ag-700	50.6	0.7	10.0	24.4	14.3
Ag-800	47.4	0.2	7.6	30.2	14.6
Ag-900	37.9	0.4	7.1	27.1	27.5

[a]Half peak width of deconvoluted peak.

DOI: 10.1021/acs.jpcc.7b10860
J. Phys. Chem. C 2018, 122, 670−680

Table 3. Percentage of Oxidized Silver Species Obtained by UV−Vis and XPS Spectra

sample	Ag-500 (%)	Ag-600 (%)	Ag-700 (%)	Ag-800 (%)	Ag-900 (%)
oxidized silver species[a]	67.7	63.7	51.3	47.6	38.3
oxidized silver species[b]	71.4	61.9	49.6	46.2	42.6

[a]Obtained by the UV−vis spectra in Table 2. [b]Obtained by the analysis of XPS spectra in Table S1.

examined (Figure 2). In the $H_2-C_3H_6-SCR$ without water vapor, both the active window for NO_x reduction and the light-off temperature of propene conversion moved to lower temperature as the calcination temperature raised. Over Ag-500, 50% NO_x conversion was obtained at the temperature of 301 °C (denoted as T_{50} hereafter, Table S2). As the calcination temperature increased, the T_{50} for NO_x conversion decreased gradually. On the Ag-900 sample, a T_{50} for NO_x conversion was obtained at 236 °C, which is 65 °C lower than that of Ag-500. Meanwhile, the T_{50} for propene conversion showed the same trend as NO_x conversion: the increase of calcination temperature significantly lowered the light-off temperature of propene. Notably, the Ag-900 obtained T_{50} for propene at 253 °C, 120 °C lower than that of Ag-500. As for Ag/Al_2O_3, high temperature calcination promoted the transformation of γ-Al_2O_3 to the δ-Al_2O_3 phase, accompanied by a decrease of surface area, which usually leads to a decrease in the deNO_x performance of HC−SCR.[13] In the present work, however, the HT-catalysts exhibited a better deNO_x activity in the absence of H_2O despite the decrease in the surface area, indicating that surface area was not the key factor in the $H_2-C_3H_6-SCR$.

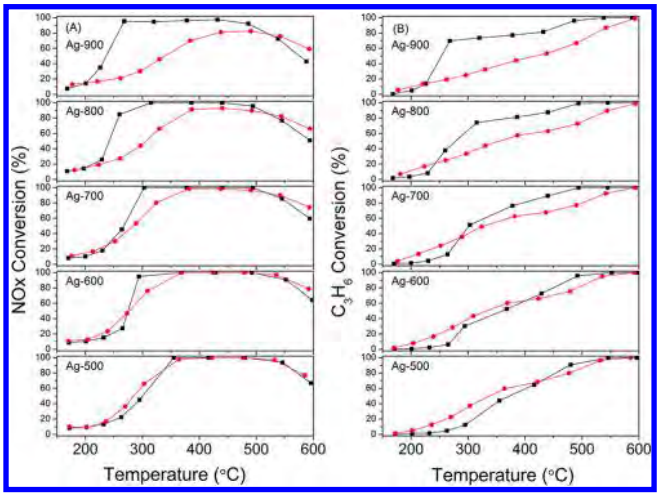

Figure 2. NO_x conversion (A) and C_3H_6 conversion (B) during $H_2-C_3H_6-SCR$ with 10% H_2O (●) or without H_2O (■) over Ag/Al_2O_3 calcined at different temperatures. Feed composition: 800 ppm of NO, 1714 ppm of C_3H_6, 1% H_2, 10% H_2O (when added), 10% O_2, N_2 balance. GHSV: 100 000 h^{-1}.

In the presence of water vapor, Ag-500 exhibited T_{50} values for NO_x and C_3H_6 conversions at 285 and 337 °C, respectively, which are even lower than those in the absence of H_2O. This promotion effect at low temperatures induced by water vapor was also observed on the Ag-600. As for the HT-catalysts, in contrast, the addition of water vapor significantly suppressed the NO_x conversion within a wide temperature range. Such deterioration was more pronounced for Ag-900, showing T_{50} values for NO_x and C_3H_6 conversions at 340 and 419 °C, respectively, which are 104 and 166 °C higher than those without H_2O in the feed.

To further confirm the distinct effects of water vapor on NO_x reduction, step-response experiments were performed at 300 °C over Ag-500 and Ag-900 (Figure 3). For better investigation of the water tolerance of Ag/Al_2O_3, the GHSV values was varied to keep the initial NO_x conversion below 90%. As for the Ag-500, the NO_x conversion increased from 37% to 61% after introduction of H_2O, while it dropped down to 32% when water vapor removed (Figure 3A). During the same process, however, the deNO_x performance of Ag-900 was significantly inhibited by H_2O addition (from 92% to 36%). In addition, the NO_x conversion on the Ag-900 continuously decreased to 60% after 3h of water removal, further confirming the suppression of water on this catalyst. Meanwhile, the water tolerance of Ag-600 was investigated in C_3H_6-SCR with 2000 ppm of H_2 (Figure S5). In this case, the Ag-600 still exhibited excellent water tolerance though the deNO_x activity was slightly lower than that with 1% H_2.

To reveal which intrinsic property determines the catalytic performance of Ag/Al_2O_3 for $H_2-C_3H_6-SCR$, the T_{50} for NO_x conversion (or C_3H_6 conversion) was further plotted against the percentage of oxidized silver species in the corresponding sample (Figure 4). Under water-free conditions, clearly, both the T_{50} values for NO_x and C_3H_6 decreased

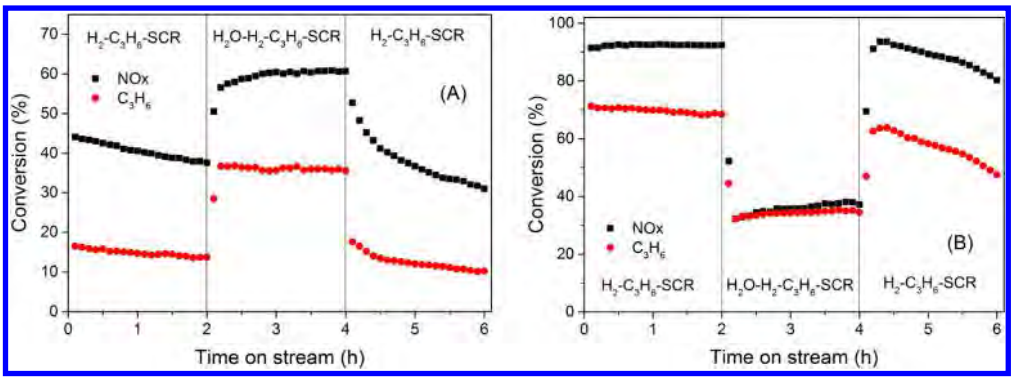

Figure 3. Step-response experiment over Ag-500 at a GHSV= 100,000 h^{-1} (A) and Ag-900 at a GHSV= 200,000 h^{-1} (B) at 300 °C in the fixed-bed reactor. Feed composition: NO, 800 ppm; C_3H_6, 1714 ppm; H_2, 1%; O_2, 10%; H_2O, 10% (when added); N_2, balance.

DOI: 10.1021/acs.jpcc.7b10860
J. Phys. Chem. C 2018, 122, 670−680

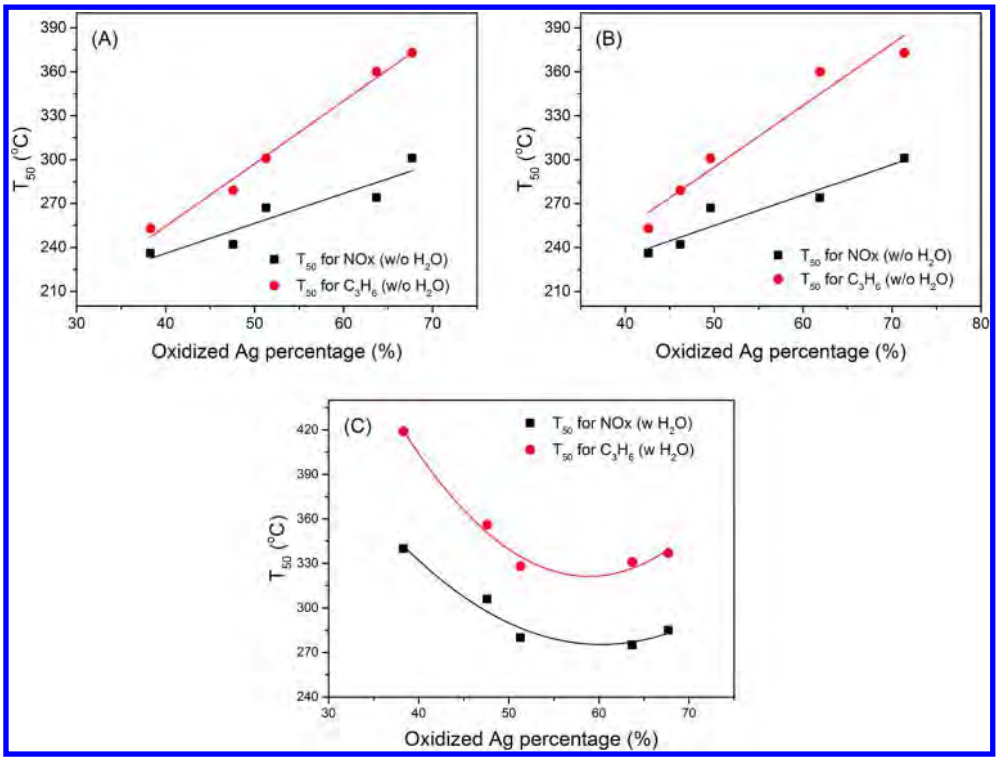

Figure 4. Relations between oxidized Ag percentage and the T_{50} for NO_x and C_3H_6 during $H_2-C_3H_6$–SCR in the absence of water vapor, with the oxidized Ag percentage obtained from UV–vis (A), and from XPS results (B), and relations between oxidized Ag percentage and the T_{50} for NO_x and C_3H_6 during $H_2-C_3H_6$–SCR in the presence of water vapor, with the oxidized Ag percentage obtained from UV–vis results (C).

linearly with the decrease of the oxidized silver percentage (Figure 4, parts A and B). Compared with the linear fitting result between T_{50} for NO_x conversion and oxidized silver percentage, a higher slope was obtained when plotting the T_{50} for C_3H_6 conversion against the oxidized silver percentage, indicating that the light-off temperature of C_3H_6 was more sensitive to the silver state.

In the presence of water vapor, however, the T_{50} values for both NO_x and C_3H_6 decreased with an increase in the percentage of oxidized silver species to 50%, which was followed by a plateau for higher oxidized silver percentages. When the percentage further increased to 65%, the deNO_x performance was even enhanced by the introduction of water vapor (Figure 4C). These results clearly suggest that an optimal percentage of oxidized silver is required for a highly efficient $H_2-C_3H_6$–SCR process. Considering that the same loading of silver was employed in all of the samples, it can be concluded that the higher the amount of oxidized silver species, the higher the water tolerance of Ag/Al_2O_3 for $H_2-C_3H_6$–SCR. However, it should be noted that, a high percentage of oxidized silver species usually resulted in a loss of low-temperature activity in the absence of water vapor. Taking the low-temperature activity and water tolerance into account, 60% oxidized silver species is therefore appropriate for $H_2-C_3H_6$–SCR.

It is well accepted that the oxidized silver species (Ag^+ and $Ag_n^{\delta+}$) are active in HC–SCR occurring on Ag/Al_2O_3 catalysts.[1−3,17,18] Recently, Nam et al.[14] systematically investigated NO_x reduction by a simulated diesel fuel-ethanol mixture over Ag/Al_2O_3 with silver loading of 1.0–6.2%. It was proposed that oxidized silver species were the active sites to reduce NO_x to N_2, while metallic silver species contributed to the partial oxidation of hydrocarbons. Hence, the presence of metallic silver species promoted the low-temperature activity for HC–SCR. As a result, an optimum oxidized/metallic ratio of silver was highly desirable for achieving high HC–SCR performance at low temperatures. Using UV–vis and XPS analysis, it was further confirmed that the optimum oxidized/metallic ratio appeared to be in the range of 1.4–1.7, which depended on the reaction temperature region. In our case, an optimal oxidized silver percentage of 60% is required for achieving high $H_2-C_3H_6$–SCR performance in the presence of water vapor, corresponding to an oxidized/metallic ratio of 1.5, which is in good agreement with the findings of Nam and co-workers.

Utilizing *n*-alkanes with different carbon numbers, Shimizu et al.[15] investigated the water tolerance of Ag/Al_2O_3 for NO_x reduction. When using *n*-octane as a reductant, notably, the presence of water vapor significantly enhanced NO_x conversion within the low temperature region. For the alkanes with carbon numbers less than 6 (i.e., *n*-C_3H_8 and *n*-C_4H_{10}), however, the deNO_x activity of Ag/Al_2O_3 was suppressed by water vapor. As a result, it was proposed that the structure of reductant has a significant effect on the deNO_x performance and water resistance of Ag/Al_2O_3. Using C_3H_6 as a reductant, herein, we found that the silver valence state also determined the water tolerance of Ag/Al_2O_3 for HC–SCR.

3.3. Activation Energy for NO_x Reduction. Activation energy measurements, as a powerful method to understand the mechanism of $H_2-C_3H_6$–SCR,[6,18,31,34,43,44] were performed over Ag/Al_2O_3 calcined at different temperatures. On the basis of the Arrhenius plots (Figure 5), the apparent activation energies (E_a) for NO_x conversion in $H_2-C_3H_6$–SCR were calculated, with the results showed in Table 4. Over all samples, the Ea values for NO_x conversion varied from 71.5 to 81.3 kJ/mol, which was in accordance with the literature.[31,43]

DOI: 10.1021/acs.jpcc.7b10860
J. Phys. Chem. C 2018, 122, 670−680

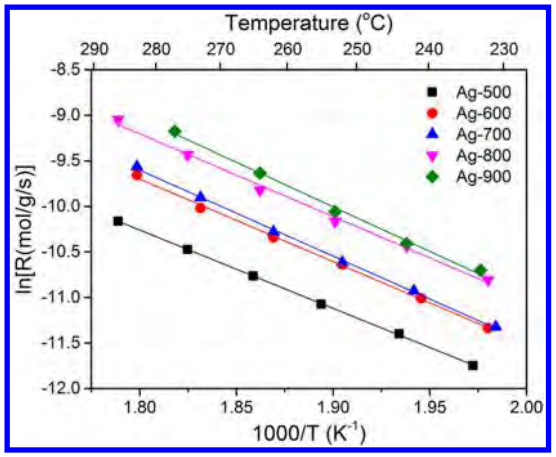

Figure 5. Arrhenius plots for the rate of NO_x conversion over Ag/Al_2O_3 catalysts during H_2−C_3H_6−SCR. Feed composition: 800 ppm of NO, 1714 ppm of C_3H_6, 10% O_2, 1% H_2, and N_2 balance. GHSV: varying in the range of 150 000−600 000 h^{-1} in order to obtain NO_x conversion below 20%.

Table 4. Apparent Activation Energy (E_a) for NO_x Conversion over Ag/Al_2O_3

sample	NO_x conversion Activation energy (kJ/mol)	reductant	ref
2% Ag/Al_2O_3 (600)	62.3	H_2 + C_3H_6	31
2% Ag/Al_2O_3 (600)	61 ± 2.5	H_2 + C_3H_8	43
Ag-500	71.5	H_2 + C_3H_6	this work
Ag-600	75.3	H_2 + C_3H_6	this work
Ag-700	78.3	H_2 + C_3H_6	this work
Ag-800	75.5	H_2 + C_3H_6	this work
Ag-900	81.3	H_2 + C_3H_6	this work

The similar Ea values for NO_x conversion indicate the same mechanism for NO_x reduction on all Ag/Al_2O_3 catalysts calcined at different temperatures. As the LT-catalysts (Ag-500 and Ag-600) and HT-catalysts (Ag-800 and Ag-900) showed distinct deNO_x performance, in situ DRIFTS experiments were performed to investigate these samples.

3.4. *In Situ* DRIFTS Studies for NO_x Reduction by C_3H_6. *3.4.1. Effect of Water Vapor on the Partial Oxidation of C_3H_6.* It is generally recognized that the partial oxidation of HCs to yield reactive intermediates is an initial process during HC−SCR over silver catalysts.[1,3,27] Hence, in situ DRIFTS studies were carried out to investigate the partial oxidation of C_3H_6 at different temperatures (Figure 6 and Figure S6). Figure 6 shows the dynamic change of adsorbed species on Ag-500 and Ag-900 during partial oxidation of C_3H_6 at 200 °C. In this process, characteristic peaks due to the intermediates of C_3H_6 partial oxidation were observed. The peaks appearing at 1577 and 1460 cm^{-1} are attributed to acetates.[10,45,46] The appearance of bands at 1591, 1394, and 1372 cm^{-1} demonstrates the formation of adsorbed formate.[24,31] According to previous studies,[11,12,34] the peaks located at 1633, 1408, and 1335 cm^{-1} are attributed to enolic species. During HC−SCR, carbonates possibly produced and adsorbed on catalyst surface, exhibiting feature FTIR peaks within the range of 1700−1300 cm^{-1}. Considering that the chemisorption of CO_2 on Al_2O_3 surface would generate carbonates,[47] the adsorption of CO_2 on Ag/Al_2O_3 had been performed in our previous study.[48] It should be noted that, the intensity of carbonates was

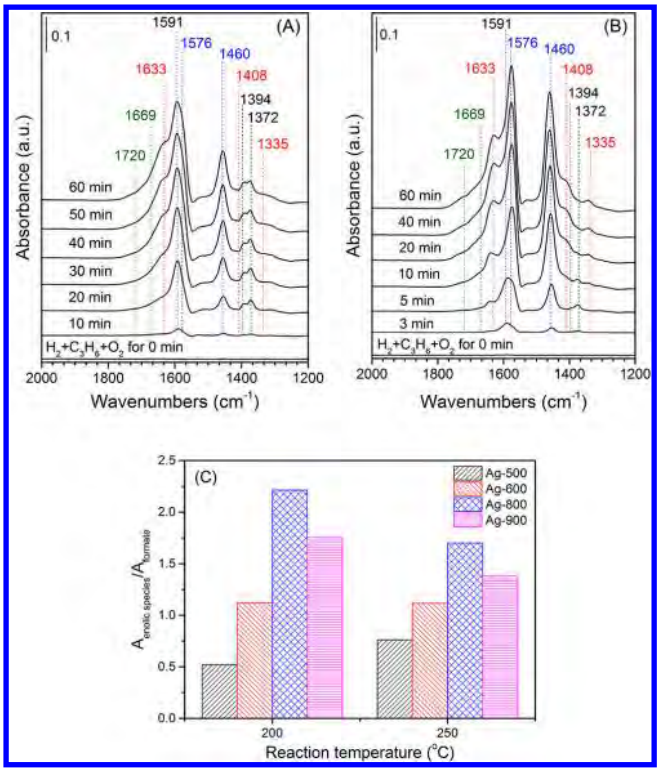

Figure 6. Dynamic change of in situ DRIFTS spectra of adsorbed species on Ag-500 (A) and Ag-900 (B) during the oxidation of C_3H_6 in the presence of H_2 at 200 °C. (C) is the integrated area ratio of enolic species (1633 cm^{-1}) to formate (1591 cm^{-1}) over LT-catalysts and HT-catalysts after exposed to H_2 + C_3H_6 + O_2 for 60 min at 200 and 250 °C (Figure S6). Feed composition: C_3H_6, 1714 ppm; H_2, 1%; O_2, 10%; N_2, balance.

much lower than those of acetate and enolic species, even when a high concentration (8 vol %) of CO_2 was employed. It indicates that, in our DRIFTS measurement for HC−SCR, the formation of carbonates is negligible, also being in agreement with the previous studies.[10,15] Meanwhile, two peaks at 1720 and 1669 cm^{-1} are attributed to the acetone.[24,31,49]

Previous results revealed that the enolic species showed high activity in the reduction of NO_x during HC−SCR on Ag/Al_2O_3,[11,34] while formate was inactive for H_2−C_3H_6−SCR.[31] At low temperatures, as these two species exhibited distinct intensities on the Ag/Al_2O_3 catalysts calcined at different temperature, it could be speculated that the formation of these two species significantly affected the light-off performance of Ag/Al_2O_3 for NO_x reduction. To this aim, the dynamic behaviors of the two species were further analyzed as discussed in the following section.

As shown in Figure 6, the peak (1591 cm^{-1}) due to formate appeared first during the partial oxidation of C_3H_6 over these samples, indicating that formate is preferentially formed or stable on the surface of Ag/Al_2O_3 catalysts.[31] As time went on, the formate on the Ag-500 (Figure 6A) increased continuously and exhibited strong intensity after reaction for 60 min. On this sample, as the adsorbed formate increased rapidly and continuously, the generation of enolic species was very slow, and thus exhibited a low intensity even after 60 min. On the Ag-900 (Figure 6B), however, the enolic species exhibited much higher formation rate compared to the formate.

In the same feed conditions, in situ DRIFTS measurement was further performed over LT-catalysts and HT-catalysts at

DOI: 10.1021/acs.jpcc.7b10860
J. Phys. Chem. C 2018, 122, 670−680

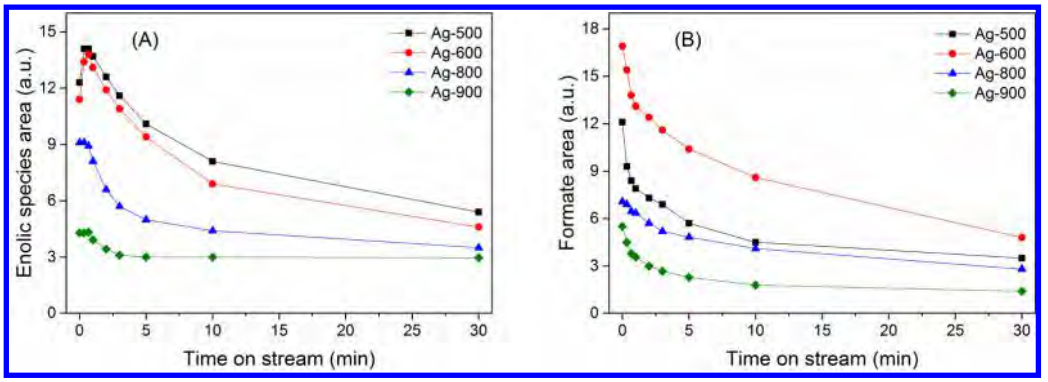

Figure 7. Dynamic changes of integrated area of the peaks due to enolic species (1633 cm^{-1}) (A) and formate (1591 cm^{-1}) (B) in the DRIFTS spectra as a function of time in a flow of $H_2O + H_2 + C_3H_6 + O_2$ at 265 °C. Before measurement, the catalyst was pre-exposed to a flow of $H_2 + C_3H_6 + O_2$ for 30 min at 265 °C. Feed composition: C_3H_6, 1714 ppm; H_2, 1%; O_2, 10%; H_2O, 5% (when added); N_2, balance.

different temperatures (Figure S6). To clarify the difference of surface intermediates over these samples, the spectra (Figure S6) were fitted and deconvoluted into their constituent peaks (with typical results presented in Figure S7). The integrated areas of peaks at 1633 cm^{-1} for enolic species and 1591 cm^{-1} for formate were obtained. At a given reaction temperature, the integrated area ratio of enolic species to formate (denoted as $A_{\text{enolic species}}/A_{\text{formate}}$ thereafter) were calculated. As shown in Figure 6C, it should be noted that, the HT-catalysts always exhibit a higher $A_{\text{enolic species}}/A_{\text{formate}}$ ratio at the reaction temperatures of 200 and 250 °C. This result suggests that the calcination of the samples at high temperature promotes the generation of enolic species while reducing the concentration of formate at low temperatures during above reaction.

The effect of water vapor on the partial oxidation of C_3H_6 was further investigated at 265 °C (Figure S8). As described above (Figure S7), the spectra (Figure S8) were fitted and deconvoluted into their constituent peaks. The corresponding integrated areas for enolic species (Figure 7A) and formate (Figure 7B) were plotted as a function of time-on-stream. On the LT-catalysts, the intensity of enolic species increased dramatically during the initial 60 s of water addition, followed by a gradual decrease in the next 30 min. On the HT-catalysts, however, the enolic species were gradually reduced during the addition of water vapor. Over all catalysts (Figure 7B), it should be highlighted that the formate was significantly inhibited by water addition, which was consistent with our previous study.[31] DFT calculation predicted that the adsorption energies of formate and enolic species on the surface of hydroxylated Ag/Al_2O_3 were less negative than those on the dehydrated surface, indicating the weaker adsorption for these species with H_2O in the feed.[31] On the LT-catalysts, as large amount of formate was eliminated by water addition, more active sites were available for the generation of enolic species, which led to a dramatic increase of enolic species in the initial 1 min. In the final stage of this experiment, however, the intensity for enolic species was lower than that without H_2O in the feed, which was due to the weaker adsorption of enolic species on the hydroxylated Ag/Al_2O_3 surface.

Generally, acidic Brønsted or Lewis oxides are suitable carriers for the development of HC−SCR catalysts, contributing to the dispersion and stabilization of active sites.[50] As a result, the acid−base property is a fundamental aspect of the activity of Ag/Al_2O_3.[51] Previous experimental and theoretical results revealed that both the Lewis acid sites (unsaturated alumina surface atoms such as Al_{IV} and Al_V sites) and the Brønsted acid sites coexist on the surfaces of pure γ-Al_2O_3 and Ag/γ-Al_2O_3.[34,52,53] As revealed by Digne et al.,[52,53] the Brønsted acid sites on γ-Al_2O_3 were derived from the dissociative adsorption of water, leading to the formation of surface hydroxyl groups while decreasing the Lewis acidity. Previous studies mentioned above also showed that the γ-Al_2O_3 was mainly enclosed by (110) and (100) planes, given the percentages of 70% and 20%, respectively. With this in mind, the adsorption energies for the formate, acetate, and enolic species were calculated on the $Ag/Al_2O_3(110)$ and $Ag/Al_2O_3(100)$.[31] On the dehydrated $Ag/Al_2O_3(110)$ surface, the DFT-calculated adsorption energies of these three species were more negative than the corresponding ones on the dehydrated $Ag/Al_2O_3(100)$ surface. Considering that the $Al_2O_3(110)$ surface exhibit stronger Lewis acidity than $Al_2O_3(100)$ plane,[53] it is possible that the Lewis acidity plays a key role in determining the adsorption of these species. However, the relationship between Brønsted acidity and the adsorption behavior of these species is hardly drawn. Taking the acetate as an example, its adsorption was weakened on the hydroxylated $Ag/Al_2O_3(110)$ surface, while enhanced on hydroxylated $Ag/Al_2O_3(100)$ one.[31]

3.4.2. Influence of H_2O on H_2−C_3H_6−SCR over Ag/Al_2O_3. In situ DRIFTS experiments of the influence of H_2O on H_2−C_3H_6−SCR over Ag/Al_2O_3 were further performed at 265 °C, with results shown in Figure 8. In this case, nitrates (1530 and 1300 cm^{-1}),[31,34] enolic species (1633 cm^{-1}), acetates (1577 and 1460 cm^{-1}), formate (1591, 1394, and 1372 cm^{-1}), acetone (1720 and 1669 cm^{-1}), and −NCO species (2230 cm^{-1}) were clearly observed. Among these species, the −NCO species is generally accepted as a key intermediate in HC−SCR.[1,2,54]

In the absence of H_2O, the peak at 1591 cm^{-1} exhibited the highest intensity on the LT-catalysts (Ag-500 and Ag-600), indicative of a strong accumulation of formate. Such accumulation of formate was more serious than that in the partial oxidation of C_3H_6 (Figure S6), confirming the formate is inactive for NO_x reduction.[31] After the introduction of water vapor into H_2+NO+C_3H_6+O_2, the peaks due to formate (1591, 1394, and 1372 cm^{-1}) on the LT-catalysts were greatly reduced, especially the peaks at 1394 and 1372 cm^{-1} totally disappeared. This result further confirmed the scavenging effect of water vapor on the formate over Ag/Al_2O_3 in H_2−C_3H_6−SCR.[31] Over the HT-catalysts, however, the formate

DOI: 10.1021/acs.jpcc.7b10860
J. Phys. Chem. C 2018, 122, 670−680

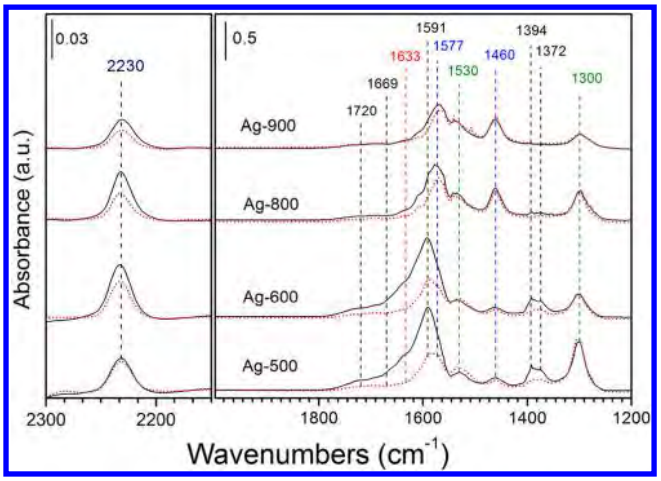

Figure 8. In situ DRIFTS spectra of adsorbed species over Ag/Al_2O_3 in a flow of $H_2O + H_2 + NO + C_3H_6 + O_2$ for 30 min (dotted line) at 265 °C. Before measurement, the catalysts were pre-exposure to $H_2 + NO + C_3H_6 + O_2$ for 30 min (solid line) at 265 °C. Feed composition: NO, 800 ppm, C_3H_6, 1714 ppm; H_2, 1%; O_2, 10%; H_2O, 5% (when added); N_2, balance.

exhibited low intensity during $H_2-C_3H_6$–SCR with or without water vapor, consistent with the results shown in Figure S8.

Figure 8 also showed that water addition decreased the intensity of peak due to enolic species (1633 cm^{-1}), particularly over the LT-catalysts. During the $H_2-C_3H_6$–SCR process, there are two possibilities contributing to the decrease of enolic species induced by water vapor: suppressing its formation and promoting its consumption by reaction with $NO + O_2$ and/or surface nitrates to form the final product of N_2. As shown in Figures 2 and 3, water vapor enhanced the low-temperature activity of LT-catalysts for NO_x reduction, while reducing the catalytic performance of HT-catalysts. This result strongly suggests that water addition enhances the consumption of enolic species in the former case. On the surface of LT-catalysts, therefore, it is reasonable that the decrease of enolic species induced by water vapor was more pronounced than that on the HT-catalysts. In this process, the reaction between acetate and $NO+O_2$ (and/or nitrates) may also contribute to NO_x reduction. Over all samples presented in Figure 8, however, the presence of water vapor hardly changes the intensity of feature peak due to acetate (1460 cm^{-1}). This result in turn, indicates that it is enolic species, rather than acetate governs the NO_x reduction at low temperatures, consistent with previous investigations.[24,27,31]

As shown in Scheme 1, the main pathway for NO_x reduction at low temperatures can be considered as follows: $NO + C_3H_6 + H_2 + O_2 \rightarrow$ ad-NO_x + enolic species $\rightarrow$ R−ONO + R-NO_2 $\rightarrow$ −NCO + −CN $\rightarrow N_2$.[1−3] Meanwhile, formate was also generated on the Ag/Al_2O_3 samples with lower silver loading, while this species showed much lower activity in the reduction of NO_x, thus accumulating on the surface and resulting in a poisoning effect.[31] The Ag/Al_2O_3 catalysts calcined at different temperatures showed quite different low-temperature activity for $H_2-C_3H_6$–SCR, while giving similar Ea values for NO_x conversion. This result indicated that the same reaction pathway occurred at low temperatures over all samples, during which the enolic species played a key role in NO_x reduction.

Scheme 1. Proposed Mechanism of $H_2-C_3H_6$–SCR over Ag/Al_2O_3

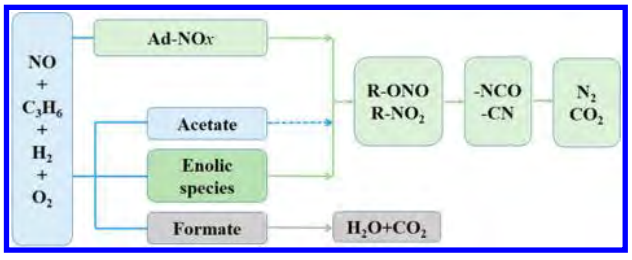

During the partial oxidation of C_3H_6, acetone, enolic species, acetate, and formate were produced over Ag/Al_2O_3 (Figures 6 and S6). The intensity of peaks due to acetone was not strong, while its formation was clearly detected by GC-MS during the same catalytic reaction.[24] Combined with our previous studies,[24,34,55] the oxidation of C_3H_6 over Ag/Al_2O_3 can be regarded as follows:

$$C_3H_6 + O_2 \rightarrow CH_3COCH_3 \quad (4)$$

$$CH_3COCH_3 + O_2 \rightarrow CH_2{=}CH - OH + HCOOH \quad (5)$$

$$CH_2 = CH{-}OH \rightarrow CH_2{=}CH{-}O^- \text{ (adsorbed on } Ag^+ \text{ sites)} + H^+ \quad (6)$$

$$HCOOH \rightarrow HCOO^- \text{ (adsorbed on } Al^{3+} \text{ sites)} + H^+ \quad (7)$$

$$CH_2{=}CH{-}O^- + O_2 \rightarrow CH_3COO^- \text{ (adsorbed on } Al^{3+} \text{ sites)} \quad (8)$$

$$HCOO^- + O_2 \rightarrow H_2O + CO_2 \quad (9)$$

Over the Ag/Al_2O_3, previous studies[9,13,18,31,34,36,56] have revealed that the silver cations (Ag^+) strongly bound to the Al sites (Ag−O−Al moieties) are the active sites for HC−SCR. The surface enolic species ($CH_2{=}CH{-}O^-$) with negative charge, which prefers to be adsorbed on these silver cations sites, exhibited higher activity to react with nitrates and/or NO_x to produce N_2 compared to acetate and formate preferentially bound to Al sites.[31,34] Considering the results presented in Figure 4A and 4B, one question may arise: why do the T_{50} values for NO_x and C_3H_6 conversions decrease linearly with an increase of metallic silver species over Ag/Al_2O_3?

Theoretical calculations also showed that the Mulliken charge of $Ag_n^{\delta+}$ was lower than that of Ag^+, the value of which decreased with an increase of the number of Ag (n).[36] This result in turn indicates that the negative enolic species prefers to bind with Ag^+ sites rather than the $Ag_n^{\delta+}$, due to a stronger electrostatic attraction in the former case. As shown in eq 6, the generation of enolic species ($CH_2{=}CH{-}O^-$) can be regarded as a process of losing a proton (H^+) from ethenol ($CH_2{=}CH{-}OH$). This process allows us to predict that the presence of neighboring electron-donating moieties would promote the formation of negative enolic species. Compared with Ag^+, the metallic silver clusters (Ag_n^0) have a higher electron density, exhibiting a higher electron donating ability. The transfer of electron from the Ag_n^0 to ethenol therefore promotes the formation of enolic species. Thus, the HT-catalysts exhibited a higher ability to form enolic species at low temperatures than the LT-catalysts, due to the higher percentage of metallic silver clusters (Figure 6 and S6). As

DOI: 10.1021/acs.jpcc.7b10860
J. Phys. Chem. C 2018, 122, 670−680

the reaction between enolic species and N-containing species is the primary pathway for NO_x reduction at low temperatures, the HT-catalysts showed a higher low-temperature activity for $H_2-C_3H_6-SCR$ without H_2O in the feed compared to the LT-catalysts (Figure 2). As indicated by eqs 4 - 7, the surface formate was derived from the dissociation and partial oxidation of acetone. Over the HT-catalysts, a higher amount of metallic silver species is beneficial for the complete oxidation of surface formate species eq 9.

Theoretical calculations and experimental measurements have shown that the (110) surface contributes ca. 70% of the total surface area of γ-Al_2O_3.[53] On this surface, DFT calculations predicted that hydroxylation decreases the adhesion energy of the metallic clusters (Pt and Pd), resulting in positive charging of the clusters.[57] In our case, hydroxylation of the support would occur on Ag/Al_2O_3 in the presence of water vapor. Such change may also positively charge the metallic silver clusters, reducing their electron-donating ability. For this reason, it could be speculated that the presence of H_2O inhibits the promotion effect of metallic silver clusters on the generation of enolic species, therefore significantly decreasing the $deNO_x$ performance of HT-catalysts. In the near future, DFT calculations involving the effect of metallic silver clusters on the generation of enolic species will be performed.

As for the LT-catalysts, the Ag^+ cations were predominant; therefore, the promotion effect of metallic silver clusters on the generation of enolic species was not pronounced compared to the HT-catalysts, while a large amount of formate was accumulated. As shown in eqs 4–7, both of these species were derived from the dissociation and partial oxidation of acetone. In this case, the accumulation of formate therefore suppressed the occurrence of the series of reactions mentioned above. In other words, the formation of enolic species was suppressed by the accumulation of formate during the $H_2-C_3H_6-SCR$, even though these two species were adsorbed on different sites of Ag/Al_2O_3. Meanwhile, a high concentration of formate would result in a strong steric effect on the generation and adsorption of enolic species. Water addition eliminated the formate, releasing the adsorption sites of Ag^+ for further reactions, eventually improving the low-temperature activity of LT-catalysts for NO_x reduction.

4. CONCLUSIONS

The valence state of silver species on Ag/Al_2O_3 played an important role in the $deNO_x$ performance and water tolerance of $H_2-C_3H_6-SCR$. High temperature calcination of Ag/Al_2O_3 promoted the transformation of oxidized silver species into metallic silver species. Oxidized silver species, particularly Ag^+, contributed to the partial oxidation of C_3H_6 to form active enolic species, serving as the active sites for the adsorption of enolic species and the reduction of NO_x. The metallic silver species promoted the generation of enolic species and the complete oxidation of formate in low temperature region, thus enhancing low-temperature activity of Ag/Al_2O_3 in the absence of water vapor. As the formate was eliminated by water addition, the $deNO_x$ performance of LT-catalysts was significantly enhanced with water in the feed. The higher the percentage of oxidized silver species, the higher the water tolerance in NO_x reduction is, indicating that the amount of oxidized silver species (overwhelmingly present as Ag^+) determines the water tolerance of Ag/Al_2O_3 for NO_x reduction. In summary, 60% oxidized silver species on Ag/Al_2O_3 catalysts is the optimal percentage for $deNO_x$ performance and water tolerance in the $H_2-C_3H_6-SCR$.

■ ASSOCIATED CONTENT

Supporting Information

The Supporting Information is available free of charge on the ACS Publications website at DOI: 10.1021/acs.jpcc.7b10860.

Details of XRD, UV–vis, XPS, XANES, activity test, and DRIFTS studies (PDF)

■ AUTHOR INFORMATION

Corresponding Authors

*Telephone: +86 10 62849121. Fax: +86 10 62849121. E-mail: ybyu@rcees.ac.cn (Y.Y.).

*Telephone: +86 10 62849123. Fax: +86 10 62849123. E-mail: honghe@rcees.ac.cn (H.H.).

ORCID

Guangyan Xu: 0000-0002-4275-7517

Yunbo Yu: 0000-0003-2935-0955

Author Contributions

The manuscript was written through contributions of all authors. All authors have given approval to the final version of the manuscript.

Funding

This work was supported by the National Key R&D Program of China (2017YFC0211105) and the National Natural Science Foundation of China (21673277 and 21637005).

Notes

The authors declare no competing financial interest.

■ REFERENCES

(1) Burch, R.; Breen, J. P.; Meunier, F. C. A Review of the Selective Reduction of NO_x, with Hydrocarbons under Lean-burn Conditions with Non-zeolitic Oxide and Platinum Group Metal Catalysts. *Appl. Catal., B* **2002**, *39*, 283–303.

(2) He, H.; Yu, Y. B. Selective Catalytic Reduction of NO_x over Ag/Al_2O_3 Catalyst: from Reaction Mechanism to Diesel Engine Test. *Catal. Today* **2005**, *100*, 37–47.

(3) Shimizu, K.; Sawabe, K.; Satsuma, A. Unique Catalytic Features of Ag Nanoclusters for Selective NO_x Reduction and Green Chemical Reactions. *Catal. Sci. Technol.* **2011**, *1*, 331–341.

(4) Miyadera, T. Alumina-supported Silver Catalysts for the Selective Reduction of Nitric Oxide with Propene and Oxygen-containing Organic Compounds. *Appl. Catal., B* **1993**, *2*, 199–205.

(5) Chaieb, T.; Delannoy, L.; Louis, C.; Thomas, C. On the Origin of the Optimum Loading of Ag on Al_2O_3 in the C_3H_6-SCR of NO_x. *Appl. Catal., B* **2013**, *142-143*, 780–784.

(6) Chaieb, T.; Delannoy, L.; Costentin, G.; Louis, C.; Casale, S.; Chantry, R. L.; Li, Z. Y.; Thomas, C. Insights into the Influence of the Ag Loading on Al_2O_3 in the H_2-assisted C_3H_6-SCR of NO_x. *Appl. Catal., B* **2014**, *156-157*, 192–201.

(7) Bartolomeu, R.; Azambre, B.; Westermann, A.; Fernandes, A.; Bertolo, R.; Hamoud, H. I.; Henriques, C.; Da Costa, P.; Ribeiro, F. Investigation of the Nature of Silver Species on Different Ag-containing NO_x Reduction Catalysts: On the Effect of the Support. *Appl. Catal., B* **2014**, *150-151*, 204–217.

(8) Valanidou, L.; Theologides, C.; Zorpas, A. A.; Savva, P. G.; Costa, C. N. A Novel Highly Selective and Stable Ag/MgO-CeO2-Al2O3 Catalyst for the Low-temperature Ethanol-SCR of NO. *Appl. Catal., B* **2011**, *107* (1–2), 164–176.

(9) Parvulescu, V. I.; Cojocaru, B.; Parvulescu, V.; Richards, R.; Li, Z.; Cadigan, C.; Granger, P.; Miquel, P.; Hardacre, C. Sol-gel-entrapped Nano Silver Catalysts-correlation between Active Silver Species and Catalytic Behavior. *J. Catal.* **2010**, *272*, 92–100.

DOI: 10.1021/acs.jpcc.7b10860
J. Phys. Chem. C 2018, 122, 670–680

(10) Sazama, P.; Capek, L.; Drobna, H.; Sobalik, Z.; Dedecek, J.; Arve, K.; Wichterlova, B. Enhancement of Decane-SCR-NO_x over Ag/alumina by Hydrogen. Reaction Kinetics and in situ FTIR and UV-vis Study. *J. Catal.* **2005**, *232*, 302−317.
(11) Yu, Y. B.; Song, X. P.; He, H. Remarkable Influence of Reductant Structure on the Activity of Alumina-supported Silver Catalyst for the Selective Catalytic Reduction of NO_x. *J. Catal.* **2010**, *271*, 343−350.
(12) Kim, P. S.; Kim, M. K.; Cho, B. K.; Nam, I. S.; Oh, S. H. Effect of H_2 on $DeNO_x$ Performance of HC−SCR over Ag/Al_2O_3: Morphological, Chemical, and Kinetic Changes. *J. Catal.* **2013**, *301*, 65−76.
(13) Yoon, D. Y.; Park, J. H.; Kang, H. C.; Kim, P. S.; Nam, I. S.; Yeo, G. K.; Kil, J. K.; Cha, M. S. $DeNO_x$ Performance of Ag/Al_2O_3 Catalyst by N-dodecane: Effect of Calcination Temperature. *Appl. Catal., B* **2011**, *101*, 275−282.
(14) Kim, M. K.; Kim, P. S.; Baik, J. H.; Nam, I. S.; Cho, B. K.; Oh, S. H. $DeNO_x$ Performance of Ag/Al_2O_3 Catalyst Using Simulated Diesel Fuel-ethanol Mixture as Reductant. *Appl. Catal., B* **2011**, *105*, 1−14.
(15) Shimizu, K.; Satsuma, A.; Hattori, T. Catalytic Performance of Ag-Al_2O_3 Catalyst for the Selective Catalytic Reduction of NO by Higher Hydrocarbons. *Appl. Catal., B* **2000**, *25*, 239−247.
(16) Sultana, A.; Haneda, M.; Fujitani, T.; Hamada, H. Influence of Al_2O_3 Support on the Activity of Ag/Al_2O_3 Catalysts for SCR of NO with Decane. *Catal. Lett.* **2007**, *114*, 96−102.
(17) Shimizu, K.; Tsuzuki, M.; Kato, K.; Yokota, S.; Okumura, K.; Satsuma, A. Reductive Activation of O_2 with H_2-reduced Silver Clusters as a Key Step in the H_2-promoted Selective Catalytic Reduction of NO with C_3H_8 over Ag/Al_2O_3. *J. Phys. Chem. C* **2007**, *111*, 950−959.
(18) She, X.; Flytzani-Stephanopoulos, M. The Role of Ag-O-Al Species in Silver-alumina Catalysts for the Selective Catalytic Reduction of NO_x with Methane. *J. Catal.* **2006**, *237*, 79−93.
(19) Satokawa, S.; Shibata, J.; Shimizu, K. I.; Satsuma, A.; Hattori, T.; Kojima, T. Promotion Effect of Hydrogen on Lean NO, Reduction by Hydrocarbons over Ag/Al_2O_3 Catalyst. *Chem. Eng. Sci.* **2007**, *62*, 5335−5337.
(20) Zhang, R. D.; Kaliaguine, S. Lean Reduction of NO by C_3H_6 over Ag/alumina Derived from Al_2O_3, AlOOH and $Al(OH)_3$. *Appl. Catal., B* **2008**, *78*, 275−287.
(21) Luo, Y. M.; Hao, J. M.; Hou, Z. Y.; Fu, L. X.; Li, R. T.; Ning, P.; Zheng, X. M. Influence of Preparation Methods on Selective Catalytic Reduction of Nitric Oxides by Propene over Silver-alumina Catalyst. *Catal. Today* **2004**, *93-95*, 797−803.
(22) Satokawa, S. Enhancing the $NO/C_3H_8/O_2$ Reaction by Using H_2 over Ag/Al_2O_3 Catalysts under Lean-exhaust Conditions. *Chem. Lett.* **2000**, *29*, 294−295.
(23) Satokawa, S.; Shibata, J.; Shimizu, K.; Satsuma, A.; Hattori, T. Promotion Effect of H_2 on the Low Temperature Activity of the Selective Reduction of NO by Light Hydrocarbons over Ag/Al_2O_3. *Appl. Catal., B* **2003**, *42*, 179−186.
(24) Yu, Y. B.; He, H.; Zhang, X. L.; Deng, H. A Common Feature of H_2-assisted HC−SCR over Ag/Al_2O_3. *Catal. Sci. Technol.* **2014**, *4*, 1239−1245.
(25) Breen, J. P.; Burch, R. A Review of the Effect of the Addition of Hydrogen in the Selective Catalytic Reduction of NO_x with Hydrocarbons on Silver Catalysts. *Top. Catal.* **2006**, *39*, 53−58.
(26) Sazama, P.; Wichterlova, B. Selective Catalytic Reduction of NO_x by Hydrocarbons Enhanced by Hydrogen Peroxide over Silver/alumina Catalysts. *Chem. Commun.* **2005**, *0*, 4810−4811.
(27) Zhang, X. L.; Yu, Y. B.; He, H. Effect of Hydrogen on Reaction Intermediates in the Selective Catalytic Reduction of NO_x by C_3H_6. *Appl. Catal., B* **2007**, *76*, 241−247.
(28) Bentrup, U.; Richter, M.; Fricke, R. Effect of H_2 Admixture on the Adsorption of NO, NO_2 and Propane at Ag/Al_2O_3 Catalyst as Examined by in situ FTIR. *Appl. Catal., B* **2005**, *55*, 213−220.
(29) Han, X.; Yu, Y. B.; He, H.; Zhao, J. J.; Wang, Y. F. Oxidative Steam Reforming of Ethanol over Rh Catalyst Supported on $Ce_{1-x}La_xO_y$ (x = 0.3) Solid Solution Prepared by Urea Co-precipitation Method. *J. Power Sources* **2013**, *238*, 57−64.
(30) Han, X.; Yu, Y. B.; He, H.; Zhao, J. J. Low CO Content Hydrogen Production from Oxidative Steam Reforming of Ethanol over CuO-CeO_2 Catalysts at Low-temperature. *J. Energy Chem.* **2013**, *22*, 861−868.
(31) Xu, G. Y.; Ma, J. Z.; He, G. Z.; Yu, Y. B.; He, H. An Alumina-supported Silver Catalyst with High Water Tolerance for H_2 Assisted C_3H_6-SCR of NO_x. *Appl. Catal., B* **2017**, *207*, 60−71.
(32) Deng, H.; Yu, Y. B.; He, H. Water Effect on Preparation of Ag/Al_2O_3 Catalyst for Reduction of NO_x by Ethanol. *J. Phys. Chem. C* **2016**, *120*, 24294−24301.
(33) Ravel, B.; Newville, M. ATHENAHE, ARTEMIS, PHAESTUS: Data Analysis for X-ray Absorption Spectroscopy Using IFEFFIT. *J. Synchrotron Radiat.* **2005**, *12*, 537−541.
(34) Yan, Y.; Yu, Y. B.; He, H.; Zhao, J. J. Intimate Contact of Enolic Species with Silver Sites Benefits the SCR of NO_x by Ethanol over Ag/Al_2O_3. *J. Catal.* **2012**, *293*, 13−26.
(35) Yu, Y. B.; Zhao, J. J.; Yan, Y.; Han, X.; He, H. A Cyclic Reaction Pathway Triggered by Ammonia for the Selective Catalytic Reduction of NO_x by Ethanol over Ag/Al_2O_3. *Appl. Catal., B* **2013**, *136-137*, 103−111.
(36) Deng, H.; Yu, Y. B.; Liu, F. D.; Ma, J. Z.; Zhang, Y.; He, H. Nature of Ag Species on Ag/gamma-Al_2O_3: A Combined Experimental and Theoretical Study. *ACS Catal.* **2014**, *4*, 2776−2784.
(37) Bethke, K. A.; Kung, H. H. Supported Ag Catalysts for the Lean Reduction of NO with C_3H_6. *J. Catal.* **1997**, *172*, 93−102.
(38) Kyriienko, P.; Popovych, N.; Soloviev, S.; Orlyk, S.; Dzwigaj, S. Remarkable Activity of Ag/Al_2O_3/cordierite Catalysts in SCR of NO with Ethanol and Butanol. *Appl. Catal., B* **2013**, *140-141*, 691−699.
(39) Strom, L.; Carlsson, P. A.; Skoglundh, M.; Harelind, H. Hydrogen-assisted SCR of NO_x over Alumina-supported Silver and Indium Catalysts Using C_2-hydrocarbons and Oxygenates. *Appl. Catal., B* **2016**, *181*, 403−412.
(40) Gunnarsson, F.; Kannisto, H.; Skoglundh, M.; Harelind, H. Improved Low-temperature Activity of Silver-alumina for Lean NO_x Reduction - Effects of Ag Loading and Low-level Pt Doping. *Appl. Catal., B* **2014**, *152-153*, 218−225.
(41) Kannisto, H.; Ingelsten, H. H.; Skoglundh, M. Ag-Al_2O_3 Catalysts for Lean NO_x Reduction-Influence of Preparation Method and Reductant. *J. Mol. Catal. A: Chem.* **2009**, *302*, 86−96.
(42) Kylhammar, L.; Palmqvist, A.; Skoglundh, M. Effects of Oxidation and Redox-properties on the Selectivity of Heat-treated Ag/Al_2O_3 Catalysts for HC−SCR of NO_x. *Top. Catal.* **2007**, *42−43*, 119−122.
(43) Shimizu, K.; Shibata, J.; Satsuma, A. Kinetic and in situ Infrared Studies on SCR of NO with Propane by Silver-alumina Catalyst: Role of H_2 on O_2 Activation and Retardation of Nitrate Poisoning. *J. Catal.* **2006**, *239*, 402−409.
(44) Richter, M.; Bentrup, U.; Eckelt, R.; Schneider, M.; Pohl, M. M.; Fricke, R. The Effect of Hydrogen on the Selective Catalytic Reduction of NO in Excess Oxygen over Ag/Al_2O_3. *Appl. Catal., B* **2004**, *51*, 261−274.
(45) Shibata, J.; Shimizu, K.; Satokawa, S.; Satsuma, A.; Hattori, T. Promotion Effect of Hydrogen on Surface Steps in SCR of NO by Propane over Alumina-based Silver Catalyst as Examined by Transient FT-IR. *Phys. Chem. Chem. Phys.* **2003**, *5*, 2154−2160.
(46) Shimizu, K.; Shibata, J.; Yoshida, H.; Satsuma, A.; Hattori, T. Silver-alumina Catalysts for Selective Reduction of NO by Higher Hydrocarbons: Structure of Active Sites and Reaction Mechanism. *Appl. Catal., B* **2001**, *30*, 151−162.
(47) Turek, A. M.; Wachs, I. E.; Decanio, E. Acidic Properties of Alumina-Supported Metal-Oxide Catalysts - an Infrared-Spectroscopy Study. *J. Phys. Chem.* **1992**, *96*, 5000−5007.
(48) Yu, Y. B.; He, H.; Feng, Q. C. Novel Enolic Surface Species Formed during Partial Oxidation of CH_3CHO, C_2H_5OH, and C_3H_6 on Ag/Al_2O_3: An in situ DRIFTS Study. *J. Phys. Chem. B* **2003**, *107*, 13090−13092.

DOI: 10.1021/acs.jpcc.7b10860
J. Phys. Chem. C 2018, 122, 670−680

(49) Zaki, M. I.; Hasan, M. A.; Pasupulety, L. Surface Reactions of Acetone on Al_2O_3, TiO_2, ZrO_2, and CeO_2: IR Spectroscopic Assessment of Impacts of the Surface Acid-base Properties. *Langmuir* **2001**, *17*, 768−774.
(50) Liu, Z. M.; Woo, S. I. Recent Advances in Catalytic $DeNO_x$ Science and Technology. *Catal. Rev.: Sci. Eng.* **2006**, *48*, 43−89.
(51) Shimizu, K.; Satsuma, A. Selective Catalytic Reduction of NO over Supported Silver Catalysts - Practical and Mechanistic Aspects. *Phys. Chem. Chem. Phys.* **2006**, *8*, 2677−2695.
(52) Digne, M.; Sautet, P.; Raybaud, P.; Euzen, P.; Toulhoat, H. Hydroxyl Groups on Gamma-alumina Surfaces: A DFT Study. *J. Catal.* **2002**, *211*, 1−5.
(53) Digne, M.; Sautet, P.; Raybaud, P.; Euzen, P.; Toulhoat, H. Use of DFT to Achieve a Rrational Understanding of Acid-basic Properties of Gamma-alumina Surfaces. *J. Catal.* **2004**, *226*, 54−68.
(54) Tamm, S.; Ingelsten, H. H.; Palmqvist, A. E. C. On the Different Roles of Isocyanate and Cyanide Species in Propene-SCR over Silver/alumina. *J. Catal.* **2008**, *255*, 304−312.
(55) Yu, Y. B.; Li, Y.; Zhang, X. L.; Deng, H.; He, H.; Li, Y. Y. Promotion Effect of H_2 on Ethanol Oxidation and NO Reduction with Ethanol over Ag/Al_2O_3 Catalyst. *Environ. Sci. Technol.* **2015**, *49*, 481−488.
(56) Deng, H.; Yu, Y. B.; He, H. Discerning the Role of Ag-O-Al Entities on Ag/gamma-Al_2O_3 Surface in NO_x Selective Reduction by Ethanol. *J. Phys. Chem. C* **2015**, *119*, 3132−3142.
(57) Hu, C. H.; Chizallet, C.; Mager-Maury, C.; Corral-Valero, M.; Sautet, P.; Toulhoat, H.; Raybaud, P. Modulation of Catalyst Particle Structure upon Support Hydroxylation: Ab initio Insights into Pd_{13} and Pt_{13}/gamma-Al_2O_3. *J. Catal.* **2010**, *274*, 99−110.

DOI: 10.1021/acs.jpcc.7b10860
J. Phys. Chem. C 2018, 122, 670−680